

See discussions, stats, and author profiles for this publication at: <https://www.researchgate.net/publication/224034648>

Enhanced Brownian Ratchet Molecular Separation Using a Self-Spreading Lipid Bilayer

ARTICLE *in* LANGMUIR · APRIL 2012

Impact Factor: 4.46 · DOI: 10.1021/la300410j · Source: PubMed

CITATIONS

13

READS

17

3 AUTHORS, INCLUDING:



Toshinori Motegi

Toyohashi University of Technology

8 PUBLICATIONS 30 CITATIONS

[SEE PROFILE](#)



Hideki Nabika

Yamagata University

58 PUBLICATIONS 697 CITATIONS

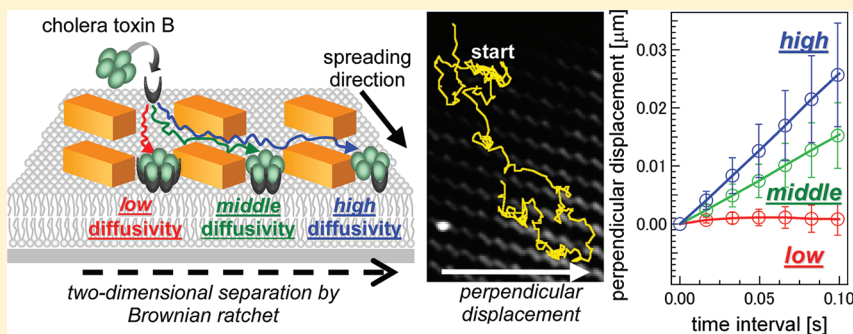
[SEE PROFILE](#)

Enhanced Brownian Ratchet Molecular Separation Using a Self-Spreading Lipid Bilayer

Toshinori Motegi, Hideki Nabika,[†] and Kei Murakoshi*

Department of Chemistry, Faculty of Science, Hokkaido University, N10W8, Kita, Sapporo 060-0810, Japan

Supporting Information



ABSTRACT: A new approach is proposed for two-dimensional molecular separation based on the Brownian ratchet mechanism by use of a self-spreading lipid bilayer as both a molecular transport and separation medium. In addition to conventional diffusivity-dependence on the ratchet separation efficiency, the difference in the intermolecular interactions between the target molecules and the lipid bilayer is also incorporated as a new separation factor in the present self-spreading ratchet system. Spreading at the gap between two ratchet obstacles causes a local change in the lipid density at the gap. This effect produces an additional opportunity for a molecule to be deflected at the ratchet obstacle and thus causes an additional angle shift. This enables the separation of molecules with the same diffusivity but with different intermolecular interaction between the target molecule and surrounding lipid molecules. Here we demonstrate this aspect by using cholera toxin subunit B (CTB)-ganglioside GM1 (GM1) complexes with different configurations. The present results will unlock a new strategy for two-dimensional molecular manipulation with ultrasmall devices.

INTRODUCTION

Innovations in molecular separation strategies with high-resolution, high-throughput, and nondestructive protocols for small quantities of biomolecules are desired for future ultrasmall devices. One typical example is the use of microscopic sieving structures. An anisotropic sieving array, which has alternating deep and shallow channels as a sieving structure,¹ enables continuous-flow separation of DNA and proteins.¹ By controlling the design of the sieving structure, diverse separation mechanisms have emerged, such as Ogston sieving,² entropic trapping,³ and electrostatic sieving.⁴ All of these strategies are candidates for molecular manipulation components in state-of-the-art small devices.

Concerning two-dimensional separation, both technological and scientific strategies have focused on a system based on the Brownian ratchet mechanism.⁵ In this mechanism, an asymmetric potential or obstacles guide the diffusing direction of the target molecules depending on their diffusive nature.^{6,7} A numerical model on the Brownian ratchet suggests that the separation angle is dependent on molecular diffusivity, i.e., molecules with different diffusivities can be separated two-dimensionally.⁸ The present ratchet system is not appropriate to separate molecules with the same diffusivity, even if they have different molecular structures or intermolecular inter-

action with the lipid bilayer. Additionally, previous systems based on ratcheting require high-energy consumption methods such as electrophoresis or water flow produced by a pump to induce the directional motion of molecules via the macroscopic flow of medium.

One possible approach to solve these limitations is the use of a self-spreading lipid bilayer as both a molecular transport and molecular separation medium.^{9–13} The self-spreading lipid bilayer can transport molecules in the bilayer in any desired direction without applying external fields such as electricity or water flow. The self-spreading is caused by a thermodynamic energy gradient from a metastable aggregate state to a stable bilayer form on the hydrated substrate. There is no need to input external energy to induce the molecular flow. Furthermore, since lipid bilayer is a main constituent of biological cell membranes, the self-spreading lipid bilayer can be used as a superior molecular transport and manipulation medium for biomolecules. It should be noted that a novel molecule filtration phenomenon has already been observed on a lipid bilayer self-spreading through nanospace.^{14,15} This

Received: January 28, 2012

Revised: March 23, 2012

Published: April 13, 2012



phenomenon is caused by a local compression of the spreading lipid bilayer in the nanospace, which alters the solubility of the doped molecule only in the nanospace. Since the solubility is reduced for a molecule that causes repulsive interaction in the compressed bilayer phase, the molecule cannot proceed into the nanospace. This retardation in the molecular transport acts as a filter for these kinds of molecules spreading through the nanospace. The parameter that determines the solubility in the compressed phase is not limited to a specific one, but widely encompasses size, charge, polarity, hydrophilicity, steric configuration, or chirality, irrespective of the diffusivity. Thus, this molecular selectivity complements the ratchet system that recognizes molecules only by diffusivity. Therefore, the incorporation of a self-spreading molecular filter into a conventional ratchet system will create a comprehensive molecular recognition and two-dimensional molecular separation method.

In the present paper, a new two-dimensional ratchet separation method was proposed by combining a self-spreading lipid bilayer and a two-dimensional ratchet substrate. A single molecule tracking observation proved that this design produced the maximum ratchet separation angle of nearly 90° for a doped molecule diffusing in the self-spreading lipid bilayer. To clarify the origin of this extremely high separation efficiency, we have developed a comprehensive model of the ratchet separation over a wide range of diffusivities, i.e., 3 orders of magnitude wider than those used in previous systems. Finally, successful differentiation in the separation angle for molecules with the same diffusivity was demonstrated by statistical analysis. All these results suggest diverse possibilities for the present system in future ultrasmall devices that can manipulate a small number of molecules without any external field.

EXPERIMENTAL PROCEDURES

Materials. 1,2-Dioleoyl-sn-glycero-3-phosphocholine (DOPC) (Avanti Polar Lipids), bovine brain ganglioside GM1 (GM1) (Avanti Polar Lipids), Alexa Fluor 555 labeled cholera toxin subunit B (CTB) (Invitrogen), and phosphate buffer solution (pH 6.8; Wako Pure Chemical Industries) were used without further purification. Water used in all of the experiments was purified by a Milli-Q system.

Substrate Fabrication. Ratchet arrays of metallic obstacles were fabricated on cleaned coverslips (Matsunami Co., Japan) by high-resolution electron beam lithography (ELS-7700H, Elionix Co., Ltd., Japan). After standard development (Zeon Co., Ltd., Japan), 5 nm chromium and 30 nm gold bilayers were deposited using a sputtering technique (ULVAC, MPS-4000, Japan). The array was composed of $250\text{ nm} \times 1\text{ }\mu\text{m}$ rectangular obstacles and placed at an angle of 45° to the lipid bilayer spreading direction (Figure 1).

Preparation of Self-Spreading Lipid Bilayer. Chloroform solutions of GM1 and DOPC were prepared at concentrations of 0.5 mg/mL and 1 mg/mL, respectively. These solutions were mixed so that the final molecular fraction was 1 mol % GM1 and 99 mol % DOPC. A small amount of the mixed solution was deposited on the substrate near the array region. After evaporating the chloroform in air, the substrate was immersed in phosphate buffer solution (pH 6.8) containing 25 mM of KH_2PO_4 and Na_2HPO_4 . Under this electrolyte condition, single lipid bilayer, not multilamellar structure, spontaneously spread from the lipid aggregate to the array region.¹⁵ CTB phosphate buffer solution was then added. The final CTB concentration was adjusted to $1.0 \times 10^{-9}\text{ M}$.

Determination of the Diffusivity of a Single Molecule. The single molecule observation for CTB was carried out with objective-type total internal reflection fluorescence microscope (TIRFM) using an IX-71 inverted microscope (Olympus). An excitation laser (532 nm, 10 mW) was delivered through an objective lens ($100 \times \text{N.A.} = 1.45$). Emission from the fluorescence dye of CTB was detected by a

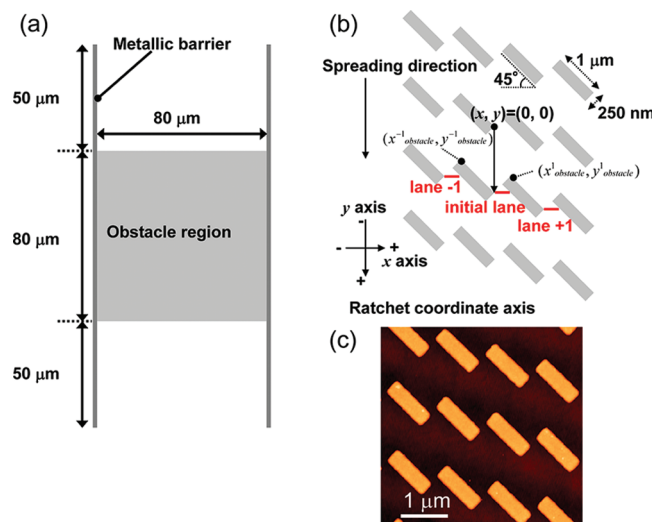


Figure 1. (a) Schematic illustration of the metallic obstacle channel. In the gray region depicted as “obstacle region”, a periodic array of ratchet obstacles shown in panels b and c was fabricated. The ratchet coordinate axis and some related information is also shown in panel b. The AFM image (c) clearly demonstrates the successful fabrication of the ratchet obstacles.

charge-coupled device (CCD) camera (C9018; Hamamatsu Photonics). The images were recorded at 60 frames/s. The molecular trajectories were obtained by recording the centers of masses of the bright spots using the Image-Pro Plus 5.1 program (Media Cybernetics). The trajectories were recorded only for molecules that maintained a constant fluorescence for more than 120 frames. Within a series of images, trajectories with diffusion coefficients of less than $0.02\text{ }\mu\text{m}^2/\text{s}$ were excluded and not used in further analyses. This exclusion avoids data uncertainty caused by enormously low diffusive molecules that may arise from nonspecific adsorption onto the metallic structures or glass substrate. Since this is not avoidable because we added excess amount of CTB molecule in the solution throughout the experiment, we eliminated the immobile fraction in the course of the diffusivity analyses.

RESULTS AND DISCUSSION

Trajectories of bright objects observed in the spreading lipid bilayer on the ratchet substrate are shown in Figure 2. In each image, the lipid bilayer spreads from the top to the bottom. Judging from the fact that each bright spot diffuses on the substrate while maintaining a constant brightness and then suddenly quenches during diffusion, each observed bright object corresponds to a single CTB molecule bound to GM1 in the bilayer (see the movie in the Supporting Information, Figure S1). This means that our tracking experiments are capable of observing single fluorescent molecules diffusing on the ratchet substrate. Furthermore, the diffusing bright spot corresponding to CTB–GM1 does not show any sudden stop near the metallic obstacles. This can rule out the adsorption of CTB–GM1 to the metallic surface (see the movie and consequent trajectory in the Supporting Information, Figure S1). Also, these trajectories show no sign of adsorption with the metal obstacles. In addition to the bright diffusing objects, scattering light from the metallic ratchet obstacles were also observed. The blurred image of the obstacles is obtained from the weak scattering light of each obstacle. By comparing four trajectories as shown in Figure 2, it is obvious that the diffusion length is highly different in the observations, i.e., CTB–GM1 in Figure 2a diffuses over only a few micrometers, whereas CTB–

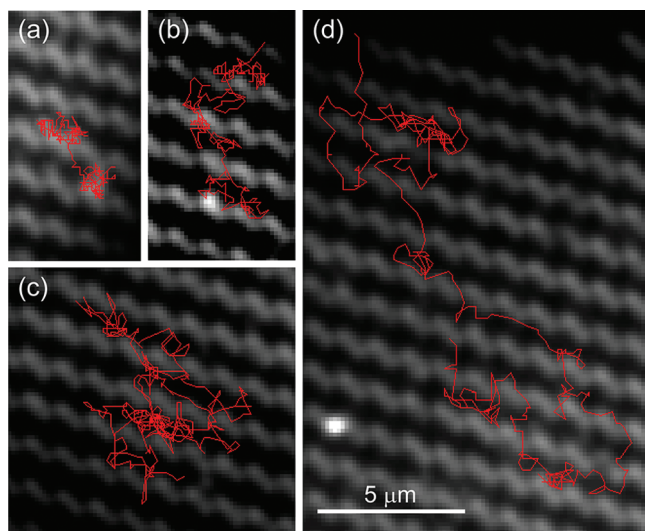


Figure 2. Typical trajectories of bright objects observed in the spreading lipid bilayer on the ratchet substrate after CTB phosphate buffer solution injection. In each image, the lipid bilayer spread from the top to the bottom. Tracking durations (t) and diffusion coefficients (D) were (a) $t = 9.6$ s, $D = 0.09 \mu\text{m}^2/\text{s}$, (b) $t = 5.4$ s, $D = 0.81 \mu\text{m}^2/\text{s}$, (c) $t = 7.4$ s, $D = 1.65 \mu\text{m}^2/\text{s}$, and (d) $t = 7.0$ s, $D = 2.99 \mu\text{m}^2/\text{s}$.

GM1 in Figure 2d diffuses over a few tens of micrometers during the same duration. This result strongly suggests the presence of several kinds of CTB–GM1 complexes with different diffusivities on the self-spreading lipid bilayer.

To quantify the CTB–GM1 diffusivity, we characterized the diffusivity by mean-square displacement analysis.¹⁶ This method enables the evaluation of diffusion coefficients (D) for each CTB–GM1 complex. The values of D from 1009 distinct trajectories are shown as a histogram in Figure 3. The

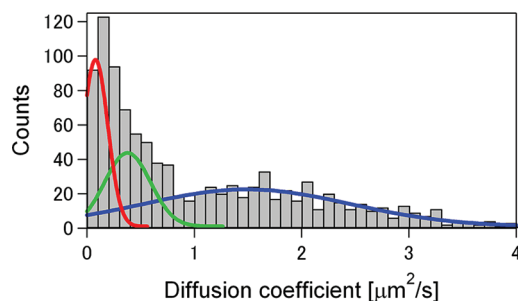


Figure 3. Diffusion coefficient histogram for molecules diffusing in the self-spreading bilayer on the ratchet substrate. The histogram was best fitted by using three Gaussian peaks centered at (red) 0.08, (green) 0.38, and (blue) $1.53 \mu\text{m}^2/\text{s}$.

histogram was best fitted by using three Gaussian curves centered at 0.08, 0.38, and $1.53 \mu\text{m}^2/\text{s}$, indicating the presence of at least three kinds of CTB–GM1 complexes with different diffusivities (the detailed analysis of fitting for diffusion histogram is shown in the Supporting Information, Figure S2). The presence of three components also appeared in the control experiment using glass substrate without metallic nano-obstacles (the diffusion coefficient histogram on glass substrate is shown in the Supporting Information, Figure S3a). The diffusion coefficients on glass substrate show slightly higher values compared with those on the ratchet substrate because of the absence of the metallic obstacles to retard the diffusion. In

order to consider the effect of nano-obstacles, hereafter we will discuss the diffusivity on the ratchet substrate. The diffusivity is dominated by the viscous dragging force, which is determined by the molecular size in the lipid bilayer.¹⁷ Since CTB has five binding sites to GM1,¹⁸ CTB can bind one to five GM1 molecules.^{19–21} The number of GM1 units in each CTB–GM1 complex determines the diffusivity, i.e., a multivalent CTB–GM1 complex with a larger number of GM1 molecules would exhibit slower diffusion.²² Although quantitative assignment between D and the binding configuration has not yet been clarified, the present result clearly demonstrates that at least three kinds of CTB–GM1 complexes with different binding configurations are formed in the self-spreading bilayer.

In addition to the random two-dimensional diffusion, the self-spreading creates directional motion for the molecule in the bilayer. Figure 4 depicts the analytical results of mean displacement for the three components observed in the diffusivity analysis. In the parallel direction, a linear increase with respect to the time interval axis was observed for both ratchet and control systems, indicating that the CTB–GM1 complex in the self-spreading lipid bilayer is effectively transported by the self-spreading.²³ However, the displacement length is strongly dependent on D , i.e., a multivalent CTB–GM1 complex that has a small D exhibits lower displacement. This would be caused by large drag friction imposed inside and outside of the bilayer for the multivalent CTB–GM1 complex.²⁴ Furthermore, the displacement on the ratchet substrate is found to be slightly lowered. The latter result suggests two roles of the metallic obstacles as barriers for the displacement. One is a role as a diffusion barrier, which reduces both diffusivity and directional displacement by a collision between diffusing molecules and obstacles. The other role is as a molecular filter created by the compressed self-spreading lipid bilayer in the nanospace, in which parallel displacement of some kinds of molecules in the self-spreading bilayer is selectively reduced.²³ Both effects contribute to the reduction of the parallel displacement on the ratchet substrate compared with the control experiment. Similar behavior was also observed in the experiment with a dye-labeled lipid as the target molecule. This indicates that both lipid and CTB–GM1 diffuse similarly in the self-spreading lipid bilayer.

On the other hand, perpendicular displacement appears only on the ratchet substrate. Negligible displacement for perpendicular direction on the control substrate is quite reasonable, because the self-spreading can transport molecules only for the direction parallel to the spreading. In other words, the self-spreading cannot offer any bias to move molecules in the perpendicular direction. In contrast, one-directional displacement for the perpendicular direction is clearly observed on the ratchet substrate. From the parallel and perpendicular displacement values on the Ratchet substrates, the separation angle for each CTB–GM1 complex were determined by a simple geometric calculation. The separation angle was plotted as a function of dimensionless diffusivity D/va ,⁸ where v and a are the flow velocity and unit cell size, respectively (Figure 5). In the present system, v is determined by the slope of the perpendicular displacement plot, and a is 250 nm. The data were shown for three groups with different diffusivity. However, as the general tendency, the separation angle shows clear and universal dependence on D/va irrespective to the diffusivity, i.e., the separation angle steeply increases at $D/va = 1$ and is saturated at the maximum separation angle of 90° at $D/va = 100$. In the intermediate region, the molecule diffuses with an

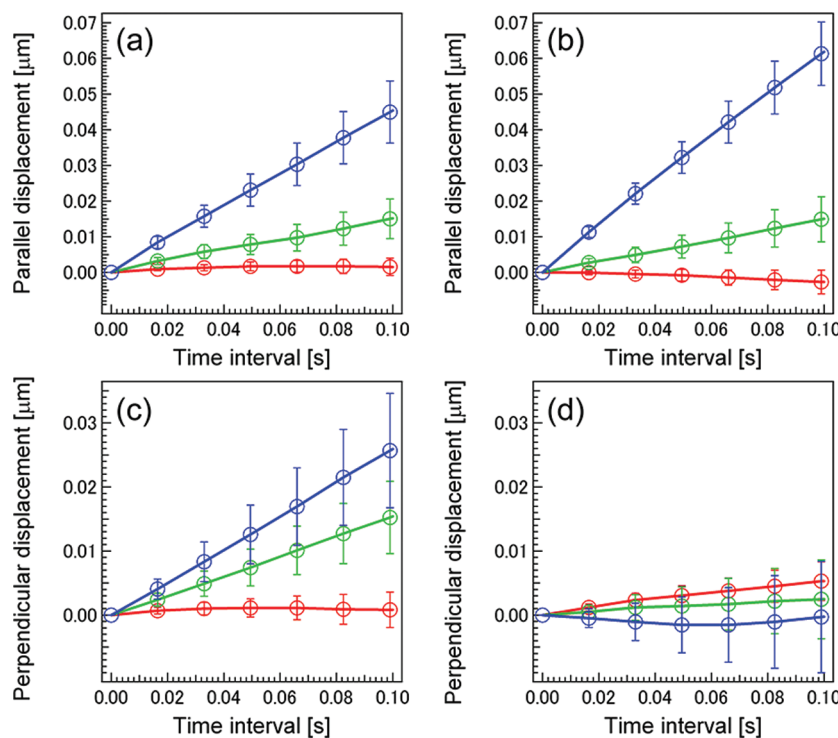


Figure 4. Averaged displacement plots of CTB-GM1 in the self-spreading lipid bilayer on the ratchet substrate (a,b) parallel and (c,d) perpendicular to the spreading direction. The plots are categorized by the diffusion coefficient of CTB-GM1: (red) 0.08, (green) 0.38, and (blue) $1.50 \mu\text{m}^2/\text{s}$. The substrates are (a,c) ratchet substrate and (b,d) control substrate without obstacles.

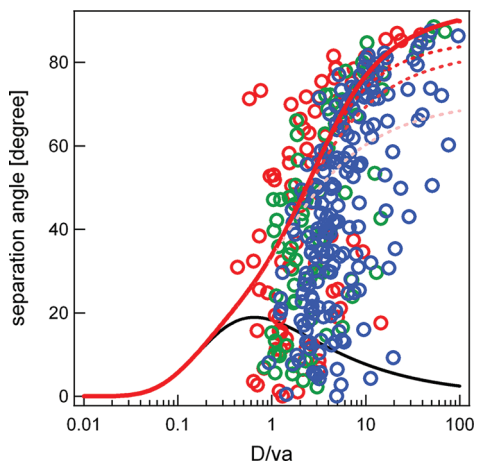


Figure 5. Ratchet separation angle plotted as a function of D/va . The plots are categorized by the diffusion coefficient of CTB-GM1: (red) 0.08, (green) 0.38, and (blue) $1.50 \mu\text{m}^2/\text{s}$, similar to Figure 4. Along with the experimental results, the previously suggested separation curve is shown (black line) as well as the modified curve considering the escaping probabilities with $i = -2$ to 5 (red line). (dot red lines, top to bottom) For comparison, the modified curves that are calculated with the escaping probabilities with $i = -1$ to 5, $i = -2$ to 3, and $i = -2$ to 2 are also drawn as dotted lines from upper to lower.

angle between 0 to 90° . This universal dependence on D/va strongly proved that the present system is working based on the ratchet model and is capable of the separation of various CTB-GM1 complexes. Furthermore, our experimental results demonstrating a separation of molecules with larger D/va values is unique compared with previous experimental⁷ and theoretical⁸ results that have demonstrated a separation of molecules with smaller D/va in the range of $0.02 < D/va < 0.3$.

With control of v and D based on the lipid bilayer composition and obstacles shape, separation with a higher degree of precision can be also achieved.

To understand these characteristic behaviors of our system, it is necessary to obtain more detail on the numerical model for the Ratchet separation. Duke et al. proposed a simple geometric solution for the molecular transport mechanism perpendicular to the flow direction based on the two-dimensional Brownian ratchet mechanism.⁸ The obstacle described in their study has the same geometrical properties as those used in our experiment, but with a different a . As the molecule was transported along the parallel direction, the probability distribution $P(x,y)$ of the molecule initially at the origin $(0,0)$ can be described with D , v , and the position coordinates (x,y) in the ratchet geometrical coordinate (see Figure 1b):

$$P(x, y) = \left(\frac{v}{4\pi Dy} \right)^{1/2} \exp\left(-\frac{x^2 v}{4Dy} \right) \quad (1)$$

In this coordination system, the spreading direction was defined as the positive- y direction, and molecules were channeled through the narrow gap between obstacles. Then, the escaping probability from the initial lane to the i th next lane due to the lateral diffusion is

$$\begin{aligned} pi &= \int_{x_{\text{obstacle}}^i}^{\infty} P(x|y_{\text{obstacle}}^i) dx \\ &= \frac{1}{2} \operatorname{erfc}\left(\sqrt{\frac{x_{\text{obstacle}}^i}{4Dy_{\text{obstacle}}^i}}\right) \\ &= \frac{1}{2} \operatorname{erfc}\left(c \times \sqrt{\frac{va}{D}}\right) \end{aligned} \quad (2)$$

where c is the constant used in the ratchet array geometry. The separation angle curve was calculated and obtained as a function of D/va by considering only the nearest-neighbor lane (black line in Figure 5). The maximum separation angle was as low as 20° and appeared at around $D/va = 0.6$, which is quite different from those observed in the present experiment. This is due to the fact that these researchers assumed that molecules diffused through gates of either $i = -1, 0$, or 1. This calculation is valid only for systems with low D/va such as electrophoresis of DNA.⁷ To improve the limit of this calculation in the higher D/va region, we modified the equation by considering the escaping probability at the i th lane as p_{sub}^i :

$$p_{sub}^i = p^i - p^{i+1}$$

$$= \int_{x_{obstacle}^i}^{\infty} P(x|y_{obstacle}^i) dx - \int_{x_{obstacle}^{i+1}}^{\infty} P(x|y_{obstacle}^{i+1}) dx \quad (3)$$

This parameter can yield the fraction of molecules passing through the i th lane, and is not limited to the nearest lanes. Although the difference in $P(x,y)$ between p^i and p^{i+1} was neglected in eq 3, this does not significantly influence our principle. In the present calculation, we mainly emphasize the importance of considering the escaping probability at not only the nearest-neighbor, but also the i th lane for the higher D/va region. Further calculations including $P(x,y)$ calibration at different p^i will improve the quantitative description of the present model.

The separation angle is then calculated with p_{sub}^i in the same way as the previously documented calculation. In the present calculation, we used the escaping probabilities with $i = -2$ to 5, since further consideration of $i < -2$ and $i > 5$ does not have any meaning because the direct diffusion into lanes with such higher i is prohibited by the geometrical configuration of ratchet obstacles. In order to consider such a geometrical condition, it is desirable to compare our experimental results and an additional numerical simulation, which is our next target.

The obtained curve as a function of D/va (Figure 5) shows good agreement with our experimental results, especially in the high D/va region. We note here that the variance in the range of i affects the separation angle in the higher D/va region, although the best fit was obtained by considering $i = -2$ to 5. Thus, the significantly high separation angle observed in the present system is explained by considering the ratchet mechanism with diffusion over lanes from -2 to 5.

The present calculation does not fully reproduce the experimental results especially in the low D/va region. This is likely due to the hydrodynamic effect that was reported in the ratchet experiment on the micrometer scale.²⁵ In our calculations, $P(x,y)$ was used for a molecule under free diffusion with a constant flow. However, the hydrodynamic flow field alters the distribution profile, especially at the gap between obstacles.^{25,26} The hydrodynamic flow forces the molecule that should be shifted toward the next lane to funnel back into the original lane. The contribution of the hydrodynamic flow caused by the spreading reduces the Ratchet separation angle especially for a molecule that is to be displaced to only one lane, i.e., a molecule with low D/va , because displacement in the perpendicular direction will be completely canceled out.

As a general tendency, the experimental results are well explained by considering the higher-order lane shift and hydrodynamic flow. In the present system, correlation between

the separation angle and D/va is quite different depending on the CTB-GM1 complex. In general, a complex with lower D gives a slightly higher separation angle (Figure 5). This tendency is more apparent when comparing the separation angle and D/va histograms of three components (Figure 6a,b).

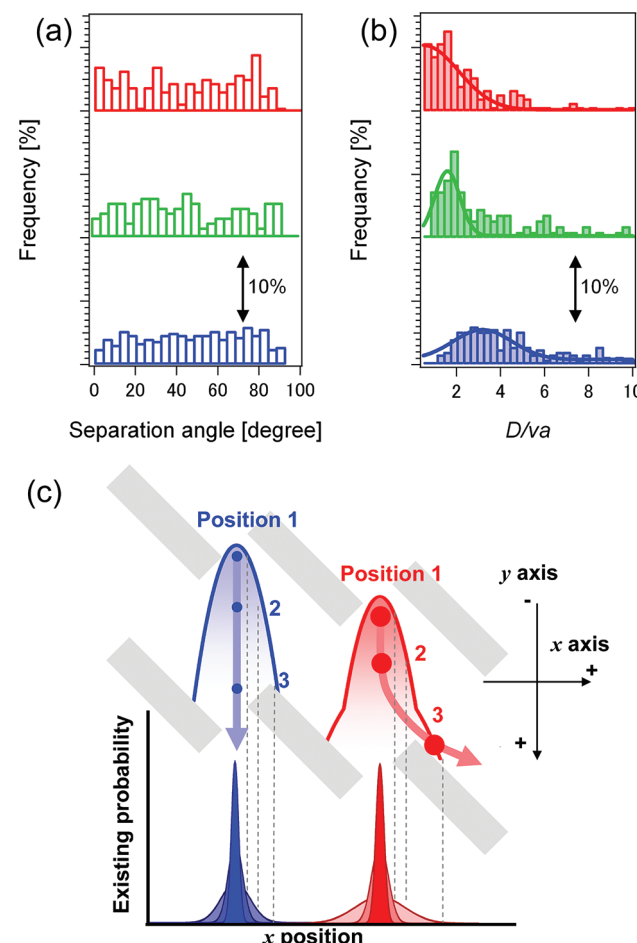


Figure 6. Distribution histograms of (a) ratchet separation angle and (b) D/va . (c) Schematic illustration of molecular distribution probability profiles. Local velocity decrease at the gap region gives an additional broadening in the distribution profiles (red) compared with normal diffusion (blue).

Although similar angle distributions are obtained for these three components, the D/va distribution shifts to a lower value for the component with low D . This implies that under the same D/va conditions the component with low D shows relatively higher separation angle, as seen in Figure 5. The observed D dependence can be explained by considering the local flow velocity decrease at the narrow gap between the obstacles.^{14,15} Normally, the molecule drifts from position 1 to position 3 by lateral diffusion (Figure 6c, left). However, the local velocity decrease at the gap causes further widening in the distribution profile. This effect provides an additional opportunity for the molecule to be shifted to the next lane during diffusion near the gap (Figure 6c, right). This effect is more evident for molecules that are structurally different from the lipid molecules, e.g., the bulky dye-labeled lipid and large multivalent protein complex. Therefore, an additional increase in the separation angle is observed for a component with large size (low D). The combination between the ratchet and the local velocity decrease

mechanisms makes it possible to create different separation angles for molecules with the same D/va but with different size, charge, polarity, hydrophilicity, or chirality, which cannot be realized only by the ratchet mechanism due to its phenomenological limitation. The present result is a promising demonstration of a versatile separation strategy that has succeeded in combining two independent separation mechanisms. Although it is necessary to take into account additional effects in the model calculations to provide a more quantitative description for the separation efficiency, the present results advance a basic principle that realizes high separation efficiency and multiple molecular recognition ability.

SUMMARY

Two-dimensional molecular separation with high separation angle was established by combining the self-spreading phenomenon and the Brownian ratchet mechanism. In order to explain the present high separation angle, we proposed a new geometrical model in the calculation, i.e., a higher-order lane shift was taken into account for molecules with high D/va . Furthermore, the use of a self-spreading lipid bilayer induced a local velocity decrease at the gap region. This system enabled the separation of molecules even with the same D/va by causing an additional ratchet shift that depended on the molecular structure. The present results unlock a new frontier of molecular separation methods that can function without an external bias but with high separation angle and higher order molecular recognition ability. This novel strategy has practical applications in microscopic and nanoscopic device technology.

ASSOCIATED CONTENT

Supporting Information

Movie for the bright object tracking in the lipid bilayer on the ratchet substrate, consequent tracking trajectory, residual plots of the fitting for the diffusion coefficient histogram, and the diffusion coefficient histogram on both the glass substrate and the ratchet substrate. This material is available free of charge via the Internet at <http://pubs.acs.org>.

AUTHOR INFORMATION

Corresponding Author

*E-mail: kei@sci.hokudai.ac.jp; phone: +81-11-706-2704.

Present Address

[†]Department of Chemistry, Faculty of Material and Biological Science, Yamagata University, Yamagata 990-8560, Japan.

Notes

The authors declare no competing financial interest.

ACKNOWLEDGMENTS

This work was partially supported by Grants-in-Aid for Scientific Research Nos. 19049003, 20750001, and 21350001 from the Ministry of Education, Science and Culture, Japan. A grant on Priority Area “Strong Photon-Molecule Coupling Fields (No. 470)” is acknowledged. T.M. also thanks the Japan Society for the Promotion of Science (JSPS) Research Fellowships for Young Scientists.

REFERENCES

- (1) Jianping, Fu; Schoch, R. B.; Stevens, A. L.; Tannenbaum, S. R.; Han, J. *Nat. Nanotechnol.* **2007**, *2*, 121.
- (2) Ogston, A. G. *Trans. Faraday Soc.* **1958**, *54*, 1754.

- (3) Muthukumar, M.; Baumgärtner, A. *Macromolecules* **1989**, *22*, 1937.
- (4) Smith, F. G.; Deen, W. M. *J. Colloid Interface Sci.* **1983**, *91*, 571.
- (5) Astumian, R. D. *Science* **1997**, *276*, 917.
- (6) van Oudenaarden, A.; Boxer, S. G. *Science* **1999**, *285*, 1046.
- (7) Chou, C.-F.; Bakajin, O.; Turner, S. W. P.; Duke, T. A. J.; Chan, S. S.; Cox, E. C.; Craighead, H. G.; Austin, R. H. *Proc. Natl. Acad. Sci. U.S.A.* **1999**, *96*, 13762.
- (8) Duke, T. A. J.; Austin, R. H. *Phys. Rev. Lett.* **1998**, *80*, 1552.
- (9) Rädler, J.; Strey, H.; Sackmann, E. *Langmuir* **1995**, *11*, 4539.
- (10) Nissen, J.; Gritsch, S.; Wiegand, G.; Rädler, J. O. *Eur. Phys. J. B* **1999**, *10*, 335.
- (11) Nissen, J.; Jacovs, K.; Radler, J. O. *Phys. Rev. Lett.* **2001**, *86*, 1904.
- (12) Suzuki, K.; Masuhara, H. *Langmuir* **2005**, *21*, 537.
- (13) Nabika, H.; Fukasawa, A.; Murakoshi, K. *Langmuir* **2006**, *22*, 10927.
- (14) Nabika, H.; Sasaki, A.; Takimoto, B.; Sawai, H.; He, S.; Murakoshi, K. *J. Am. Chem. Soc.* **2005**, *127*, 16786.
- (15) Nabika, H.; Iijima, N.; Takimoto, B.; Ueno, K.; Misawa, H.; Murakoshi, K. *Anal. Chem.* **2009**, *81*, 699.
- (16) Saxton, M. J. *Biophys. J.* **1993**, *64*, 1766.
- (17) Guigas, G.; Weiss, M. *Biophys. J.* **2006**, *91*, 2393.
- (18) Merritt, E. A.; Sarfati, S.; van den Akker, F.; L'hoir, C.; Martial, J. A.; Hol, W. G. J. *Protein Sci.* **1994**, *3*, 166.
- (19) Schön, A.; Freire, E. *Biochemistry* **1989**, *28*, 5019.
- (20) Lauer, S.; Goldstein, B.; Nolan, R. L.; Nolan, J. P. *Biochemistry* **2002**, *41*, 1742.
- (21) Shi, J.; Yang, T.; Kataoka, S.; Zhang, Y.; Diaz, A. J.; Cremer, P. S. *J. Am. Chem. Soc.* **2007**, *127*, 16786.
- (22) Forstner, M. B.; Yee, C. K.; Parikh, A. N.; Groves, J. T. *J. Am. Chem. Soc.* **2006**, *128*, 15221.
- (23) Takimoto, B.; Nabika, H.; Murakoshi, K. *Nanoscale* **2010**, *2*, 2591.
- (24) Burns, A. R.; Frankel, D. J.; Buranda, T. *Biophys. J.* **2005**, *89*, 1081.
- (25) Huang, L. R.; Silberzan, P.; Tegenfeldt, J. O.; Cox, E. C.; Strum, J. C.; Austin, R. H.; Craighead, H. *Phys. Rev. Lett.* **2002**, *89*, 178301.
- (26) Austin, R. H.; Darnton, N.; Huang, R.; Sturm, J.; Bakajin, O.; Duke, T. *Appl. Phys. A: Mater. Sci. Process.* **2002**, *75*, 279.